



Hierarchical NiCo₂S₄@Ni₃S₂ core/shell nanorod arrays supported on carbon cloth for all-solid-state flexible asymmetric supercapacitors

Jiang Zhan^{1,3} · Lina Shan² · Yanwei Sui^{1,3} · Jiqiu Qi¹ · Fuxiang Wei¹ · Yezeng He¹ · Qingkun Meng¹ · Zhi Sun¹ · Jinlong Liu¹

Received: 19 January 2019 / Accepted: 19 June 2019 / Published online: 4 July 2019
© Springer Science+Business Media, LLC, part of Springer Nature 2019

Abstract

Flexible electrodes for preparing core–shell structures are receiving increasing attention. A composite electrode material with NiCo₂S₄ as the core and Ni₃S₂ as the shell was successfully synthesized by hydrothermal synthesis and electrodeposition method. The prepared flexible NiCo₂S₄@Ni₃S₂ core/shell nanorod array has higher electrochemical performance, with specific capacitance of 5.714 F cm⁻² at 2 mA cm⁻² and excellent cycle stability. In addition, the prepared flexible hybrid supercapacitor has been assembled with NiCo₂S₄@Ni₃S₂ as the positive electrode and Fe₂O₃-rGO as the negative electrode, delivering an energy density of 5.9 mWh cm⁻³ at 171 mW cm⁻³. These results make the NiCo₂S₄@Ni₃S₂ a high-performance supercapacitor application candidate.

1 Introduction

The role of renewable energy as a potential substitute for fossil fuels in energy storage equipment has drawn attention in the past few decades. Looking for an energy storage device has become an urgent problem to be solved [1–4]. Among various energy storage devices, supercapacitors can cope with this huge challenge due to its high power density, long service life, and fast charge/discharge rate [5, 6]. Nowadays, Exploring new electrode materials is critical to improving the electrochemical performance of supercapacitors [7]. In general, the electrode materials of supercapacitors are divided into two categories: electrical double-layer capacitors and pseudocapacitors [8]. It has been believed that pseudocapacitors have higher energy specific capacitance and

energy density due to their rich redox reaction and active site, which has attracted increasing attention in energy storage [9, 10], such as MnO₂ [11–13], Co₃O₄ [14, 15], Fe₂O₃ [16, 17].

Recently, metal sulfides including NiCo₂S₄ [18–21], MnCo₂S₄ [22–24], FeCo₂S₄ [25, 26], Ni₃S₂ [27–29] and CoS [30] have become one of the most promising electrode materials for supercapacitors because of their high theoretical capacitance, low cost, and simple preparation methods [31, 32]. For example, Lin et al. have successfully fabricated the P-doped NiCo₂S₄ nanotube arrays, which exhibits high specific capacitance of 8.03 F cm⁻² at 2 mA cm⁻² and 87.5% capacitance retention after 5000 cycles [33]. Li et al. have synthesized the NiCo₂S₄@Co(OH)₂ core–shell nanotube arrays on Ni foam by an easy-to-use method with excellent electrochemical performance of 9.6 F cm⁻² at 2 mA cm⁻² compared with bare NiCo₂S₄ electrode [34]. Yang et al. prepared the NiCo₂S₄@MnO₂ heterostructure by a simple strategy. The NiCo₂O₄@MnO₂ has a high specific capacitance of 1337.8 F/g at a current density of 2.0 A/g compared to pure NiCo₂S₄ [21]. Xianbin Liu et al. used a hydrothermal method and potentiostatic deposition method to synthesize unique heterostructure of PANI shell cladding on core NiCo₂S₄ nanowires that showed areal capacitance of 4.74 F cm⁻² at 2 mA cm⁻² and a capacitive retention of 86.2% after 5000 cycles [35]. This single NiCo₂S₄ usually does not achieve optimum performance due to incomplete redox reactions and insufficient contact of the active material

✉ Yanwei Sui
wyds123456@outlook.com

✉ Jinlong Liu
liujlong@cumt.edu.cn

¹ School of Materials Science and Engineering, China University of Mining and Technology, Xuzhou, People's Republic of China

² School of Material, Harbin University of Science and Technology, Harbin, People's Republic of China

³ The JiangSu Province Engineering Laboratory of High Efficient Energy Storage Technology and Equipments, Xuzhou 221116, People's Republic of China

with the electrolyte [21]. Therefore, it is believed that the synergy produced by the core–shell structure can solve these problems. Obviously, the method of improving the performance of the electrode material by preparing such a core–shell structure combined with different electrode materials has greater application potential for the supercapacitors [12, 36, 37].

The present work is mainly focused on prepared Ni₃S₂ film on NiCo₂S₄ to form a core–shell structure by two-step hydrothermal and electrodeposition method, with specific capacitance of 5.714 F cm⁻² at 2 mA cm⁻². The flexible asymmetric supercapacitor device is composed of NiCo₂S₄@Ni₃S₂ core/shell as a positive electrode and Fe₂O₃-rGO as a negative electrode, which exhibits high energy and power density. The results show that NiCo₂S₄@Ni₃S₂ core/shell nanorod arrays has great application value in high performance capacitors.

2 Experimental section

2.1 Materials

The urea, CoCl₂·6H₂O, NiCl₂·6H₂O, Na₂S·9H₂O, KMnO₄, and NH₄F (Aladdin Reagent Co, Shanghai, China) were of analytical grade and used without any further purification conditions. Graphene oxide was synthesised with a modified Hummers method and the reduced GO was obtained by thermal reduction [38, 39].

2.2 Synthesis of NiCo₂S₄ on carbon cloth

First of all, the commercial carbon cloth (1 cm × 2 cm × 1.6 mm) was cleaned carefully with 0.5 mol/L potassium permanganate solution (Oxidant), ethanol and deionized water in an ultrasonic cleaning instrument for 15 min to remove impurities from the surface. Then, it was dried in vacuum at 70 °C for 12 h. The NiCo₂S₄ nanorod supported on carbon fiber cloth were prepared via two-step hydrothermal reaction. Firstly, 2 mmol NiCl₂·6H₂O, 4 mmol CoCl₂·6H₂O, 10 mmol urea and 2.7 mmol NH₄F were dissolved in 40 mL DI water with stirring to form claret-red solution. The solution was transferred to a 50 mL Teflon-lined stainless steel autoclave and the carbon cloth was then added and maintained at 120 °C for 6 h. The resulting products were cooled down to room temperature and collected by washing with DI water and ethanol, then dried in the oven at 60 °C for 12 h. Secondly, the precursor was distributed into 40 mL 0.2 M Na₂S·9H₂O water solution and heated to 160 °C for 8 h. After cooling to ambient temperature, the NiCo₂S₄ supported on carbon cloth was rinsed with deionized water and ethanol, and dried under vacuum at 70 °C for 12 h. The mass of NiCo₂S₄ is about 7.55 mg cm⁻².

2.3 Synthesis of NiCo₂S₄@Ni₃S₂ core/shell nanorod arrays

We used a potentiostatic deposition method to synthesize Ni₃S₂ on the surface of NiCo₂S₄ nanorod arrays. First, 1 mol thiourea and 2.5 mol NiCl₂·6H₂O were dissolved in 50 mL of distilled water and stirred for half an hour by magnetic stirring. In a typical electrodeposition process, the NiCo₂S₄ nanorod sample electrode was used as the working electrode in the prepared solution, the platinum electrode used as the counter electrode, and the Hg/HgO as the reference electrode by cyclic voltammetry within the potential range of -1.2 V to 0.2 V with a sweep rate of 5 mV/s for 2 cycles, 5 cycles and 8 cycles, respectively. The obtained samples were washed with distilled water and absolute ethanol and then dried under vacuum at 70 °C for 12 h. After calculation, the mass of 5-NiCo₂S₄@Ni₃S₂ is about 1.175 mg cm⁻².

2.4 Synthesis of the Fe₂O₃-rGO

Fe₂O₃-rGO hydrogel was synthesized by the following process. 1 mmol FeCl₃·6H₂O were dispersed in 30 mL GO dispersion under ultrasonication for 30 min to form homogeneous solution. Next, the obtained homogeneous solution was transferred into a 50 mL Teflon-lined stainless-steel autoclave, and maintained at 180 °C for 12 h. The resulting sample was washed with DI water and absolute ethanol for several times, and dried under vacuum at 70 °C for 12 h. The prepared active material, acetylene black, polyvinylidene fluoride (PVDF) and 1-methyl-2-pyrrolidone (NMP) were mixed at a mass ratio of 8:1:1 and stirred for 1 h to form uniform slurry. Subsequently, in order to better bond the active material to the carbon cloth, a conductive carbon paste was applied before the slurry was brushed on the carbon cloth, and then dried at 70 °C for 12 h.

2.5 Fabrication of asymmetric supercapacitor

The solid-state asymmetric supercapacitor device was assembled by using NiCo₂S₄@Ni₃S₂ Fe₂O₃/rGO and PVA-KOH gel as positive, negative electrodes and electrolyte, respectively. The energy density (E), and power density (P), were calculated according to the following equations [12, 40].

$$E = \frac{1}{2 \times 3600} C_{ASC} \times \Delta V^2, \quad (1)$$

$$P = \frac{E}{\Delta t} \times 3600, \quad (2)$$

where Δt (s) is the discharge time, C_{ASC} (mF cm⁻²) is the electrochemical performance, ΔV (V) is the potential window of the device, E (mWh cm⁻³) is energy density and P (mW cm⁻³) is power density.

3 Material characterization

The structural and compositions of samples were recorded by X-ray diffractometer (XRD, D8 Advance, Bruker, Germany). A FEI Tecnai G² F20 transmission electron microscopy (TEM) and SU8220 scanning electron microscope (SEM) were used to further investigate the microstructure and morphology of synthesized products.

4 Electrochemical measurement

The electrochemical performances of the products were investigated in the electrochemical workstation (Shanghai Chenhua Instruments, CHI660D) in a standard three-electrode configuration with 2 M KOH solution as electrolyte. The sample was directly used as the working electrode, while a Hg/HgO electrode and platinum foil were employed as the reference electrode and counter electrode, respectively. Cyclic voltammetry (CV) and galvanostatic charge–discharge (GCD) measurements were used to study the electrochemical performance of the NiCo₂S₄@Ni₃S₂ core/shell nanorod arrays. In addition, electrochemical impedance spectroscopy (EIS) tests were conducted in the frequency range of 0.01 kHz to 100 Hz with an amplitude of 5 mV.

5 Results and discussion

5.1 Structural and morphological characterization

The corresponding schematic illustration for the fabrication of the hierarchical NiCo₂S₄@Ni₃S₂ core/shell nanorod arrays supported on carbon cloth (CF) is as shown in Fig. 1.

Fig. 1 Schematic illustration of the formation of the NiCo₂S₄@Ni₃S₂

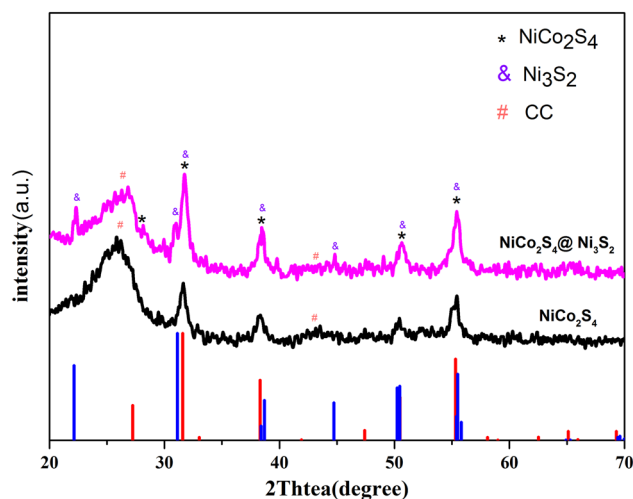
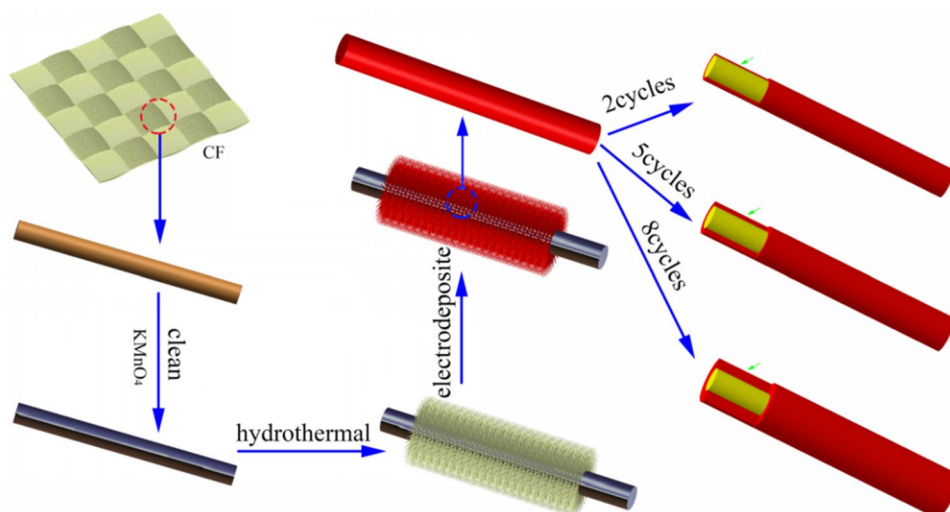


Fig. 2 XRD patterns of the NiCo₂S₄@Ni₃S₂ and NiCo₂S₄

Initially, the carbon cloth was washed with potassium permanganate, and NiCo₂S₄ nanotubes were prepared by hydrothermal method. Next, the hierarchical NiCo₂S₄@Ni₃S₂ core/shell nanorod arrays were obtained by electrodeposition method. At the same time, the influence of the different CV cycles on the composite during the electrodeposition process was shown. This kind of hierarchical NiCo₂S₄@Ni₃S₂ core/shell nanorod arrays structure, decrease the electrolyte ion transportation path during the charge/discharge process [41].

Figure 2 shows the XRD traces of NiCo₂S₄ and NiCo₂S₄@Ni₃S₂. As observed, the diffraction peaks at 2θ values of 26.83, 31.59, 33.03, 38.32, 47.41, 50.46 and 55.33 correspond to the (2 2 0), (3 1 1), (2 2 2), (4 0 0), (4 2 2), (5 1 1) and (4 4 0) planes of NiCo₂S₄ (JCPDS No. 20-0782). After the electrodeposition reaction, the obtained NiCo₂S₄@Ni₃S₂ shows diffraction peaks at 2θ values of 21.98, 31.19,

38.49, 38.77, 44.82, 50.35, 50.57, 55.51, 55.62 and 55.94 can be well indexed to the (0 1 0), (−1 1 0), (−1 1 1), (1 1 1), (0 2 0), (−1 2 0), (1 2 0), (−2 1 1), (−1 2 1) and (1 2 1) crystal planes of Ni_3S_2 (JCPDS No. 85-0775). While the other two obvious characteristic peaks belong to carbon cloth, these results suggest the successful formation of high purity of $\text{NiCo}_2\text{S}_4@ \text{Ni}_3\text{S}_2$ core/shell nanorod arrays in the composite.

The basic composition of composite 5- $\text{NiCo}_2\text{S}_4@ \text{Ni}_3\text{S}_2$ and the chemical price of different elements were further characterized by X-ray photoelectron spectroscopy (XPS) in Fig. 3. Figure 3a shows the Ni Co, S, N, O, and C elements, which correspond to the elements of the 5- $\text{NiCo}_2\text{S}_4@ \text{Ni}_3\text{S}_2$ sample. The four fitted peaks are shown in Fig. 3b by high resolution Ni 2p spectra, with two peaks centered at 872.7 and 854.1 eV corresponding to the Ni^{2+} signal, while the other two peaks are at 855.9 and 873 eV belong to the Ni^{3+} and two shake-up satellites (denoted as “Sat.”) [42]. For the Co 2p high resolution XPS spectrum in Fig. 3c could also

be fitted to two spin–orbit doublets, which are characteristic of Co^{2+} and Co^{3+} , and two shake-up satellites [43]. Furthermore, the peaks at 163.4 eV and 163.4 eV in the high-resolution S 2p spectrum are identified as S^{2-} in Fig. 3d [44]. The above XPS analysis results show that $\text{NiCo}_2\text{S}_4@ \text{Ni}_3\text{S}_2$ contains cationic Ni^{3+} , Ni^{2+} , Co^{2+} , Co^{3+} and S^{2-} , which provide abundant active sites for energy storage [45].

Figure 4 shows SEM images at different magnifications of NiCo_2S_4 nanorod arrays morphology, revealing that all NiCo_2S_4 exhibit nanorod arrays morphology with a uniform size distribution. After the treatment with electrodeposition, a large number of Ni_3S_2 membrane structures grow on the surface of NiCo_2S_4 , resulting in the surface of the NiCo_2S_4 nanorod wrapped by the Ni_3S_2 layer. The obtained $\text{NiCo}_2\text{S}_4@ \text{Ni}_3\text{S}_2$ core/shell nanorod arrays were still uniformly arranged on a large scale on a carbon cloth. To investigate into the structure change of $\text{NiCo}_2\text{S}_4@ \text{Ni}_3\text{S}_2$ core/shell nanorod arrays at different CV cycles stages, the corresponding SEM images were collected in Fig. 5. It is worth noting

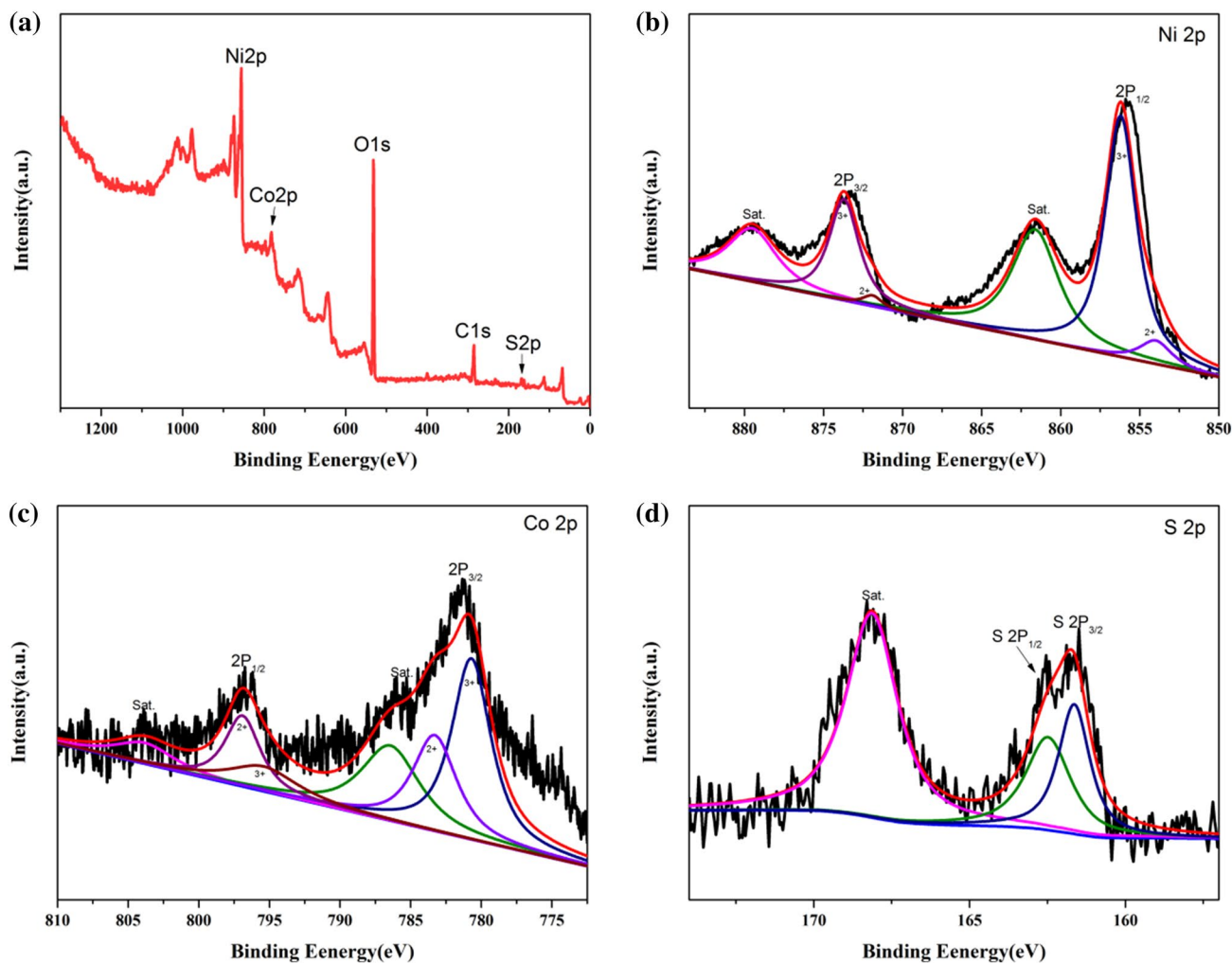


Fig. 3 XPS analysis of wide scans of **a** $\text{NiCo}_2\text{S}_4@ \text{Ni}_3\text{S}_2$ sample, and narrow scans of **b** Ni 2p, **c** Co 2p, **d** S 2p

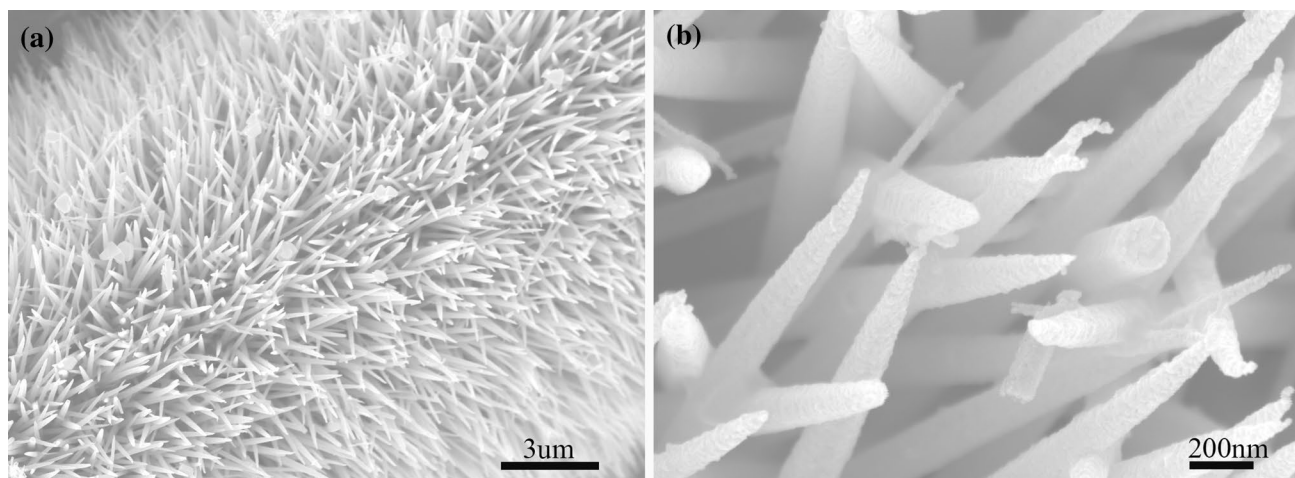


Fig. 4 a, b SEM images of the NiCo₂S₄ under different magnifications

that the thickness of the Ni₃S₂ shell can be easily increased by prolonging the electrodeposition reaction time.

Figure 5 shows the effect of different CV cycles on morphology and it can be clearly observed that the thickness of Ni₃S₂ increases as the CV cycle increases from 2 to 8 cycles. As shown in Fig. 5c, for the sample 2-NiCo₂S₄@Ni₃S₂ treated with electrodeposition cycles, a small amount

of the Ni₃S₂ film is partially dispersed at the outer end of the rod-shaped NiCo₂S₄. As the number of electrodeposition cycles increases in Fig. 5a and b, the Ni₃S₂ film of 5-NiCo₂S₄@Ni₃S₂ sample with five electrodeposition cycles become thicker and the coverage of the Ni₃S₂ nanosheets increases, eventually a nanomembrane shape structure and uniformly anchored on the surface of the NiCo₂S₄. In

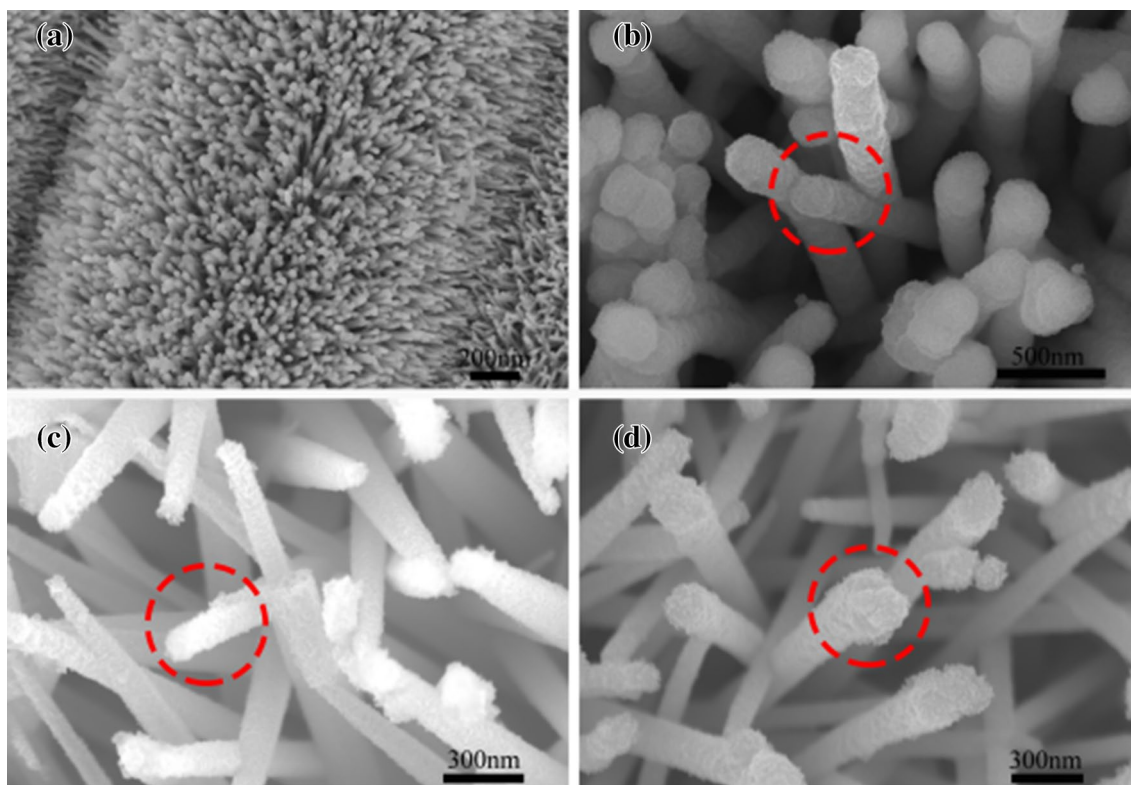


Fig. 5 a, b SEM images of the 5-NiCo₂S₄@Ni₃S₂ under different magnifications. c SEM images of the 2-NiCo₂S₄@Ni₃S₂. d SEM images of the 8-NiCo₂S₄@Ni₃S₂

Fig. 5d, as the number of electrodeposited turns increase to 8 cycles, the thickness of sample 8-NiCo₂S₄@Ni₃S₂, becomes much higher, resulting in over-stacked. The NiCo₂S₄@Ni₃S₂ core/shell nanorod arrays structures are favorable for electrolyte penetration and increasing the electrode/electrolyte contact area, resulting in enhanced electrochemical performance [21, 36].

The structure and morphological change of the NiCo₂S₄@Ni₃S₂ core/shell nanorod arrays were further investigated using TEM in Fig. 6. For the NiCo₂S₄@Ni₃S₂ core/shell nanorod arrays, low magnification TEM images show NiCo₂S₄ species morphology and surface loading of Ni₃S₂. As shown in Fig. 6b–d, the thickness of Ni₃S₂ can be easily changed by controlling the number of CV cycles. It is apparent that when the number of electrodeposition cycles is 5 cycles, the NiCo₂S₄ nanorods are completely covered by a Ni₃S₂ layer within a thickness of approximately 20 nm forming a typical core–shell structure. The TEM image also further indicates that the thickness of the 5-NiCo₂S₄@Ni₃S₂

is uniform, while the 2-NiCo₂S₄@Ni₃S₂ are too thin and 8-NiCo₂S₄@Ni₃S₂ are too thick, these changes may be the cause of changes in electrochemical performance.

5.2 Electrochemical characterization

To explore electrochemical properties of NiCo₂S₄ nanorod arrays and NiCo₂S₄@Ni₃S₂ core/shell nanorod arrays as electrodes, cyclic voltammetry (CV) and galvanostatic charge–discharge tests (GCD) of the synthesized samples were performed with a three-electrode cell in the 2 M KOH aqueous electrolyte. Figure 7a shows the CV curves of NiCo₂S₄ and NiCo₂S₄@Ni₃S₂ core/shell nanorod arrays electrodes at a scan rate of 30 mV s⁻¹. In each curve, a pair of redox peaks are clearly observed in the voltage range of -0.3 V and 0.9 V, respectively. As shown in Fig. 7a, it is easily observed that the integral area of NiCo₂S₄@Ni₃S₂ CV curve is much larger, implying fast electrochemical redox reaction and higher electrochemical energy storage

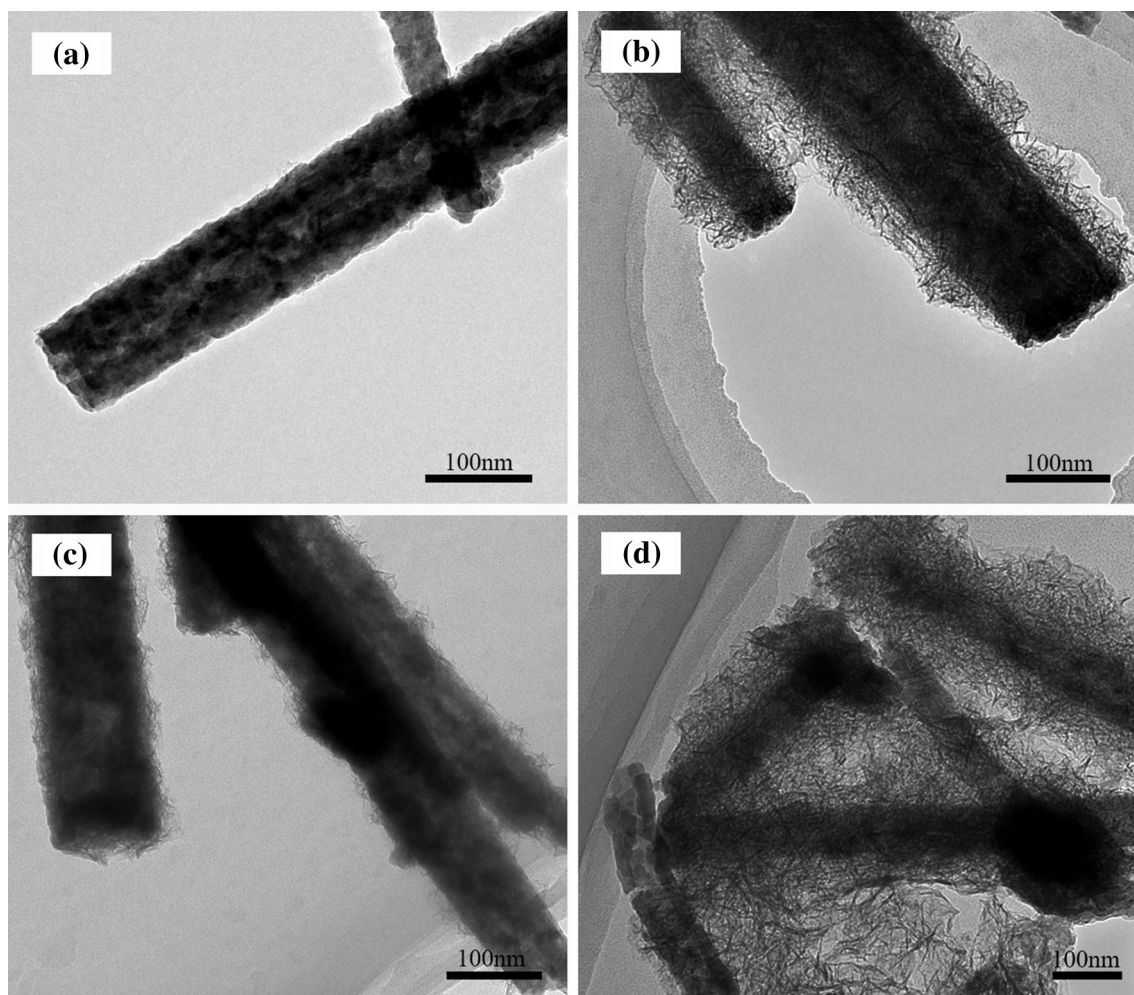


Fig. 6 **a, b** TEM images of the 5-NiCo₂S₄@Ni₃S₂ under different magnifications. **c** TEM images of the 2-NiCo₂S₄@Ni₃S₂. **d** TEM images of the 8-NiCo₂S₄@Ni₃S₂

capacity [23]. Figure 7b shows the CV curve of NiCo_2S_4 @ Ni_3S_2 core/shell nanorod arrays in 2 M KOH aqueous solution at different scan rates in a potential window of -0.3 to 0.9 V. All curves have significant redox peaks in the CV

curve, indicating that the fast and reversible electrochemical redox reaction processes occur at the electro-active material/electrolyte [11]. In addition, as the scanning rate increases, the current density increases and the shape of the curve does

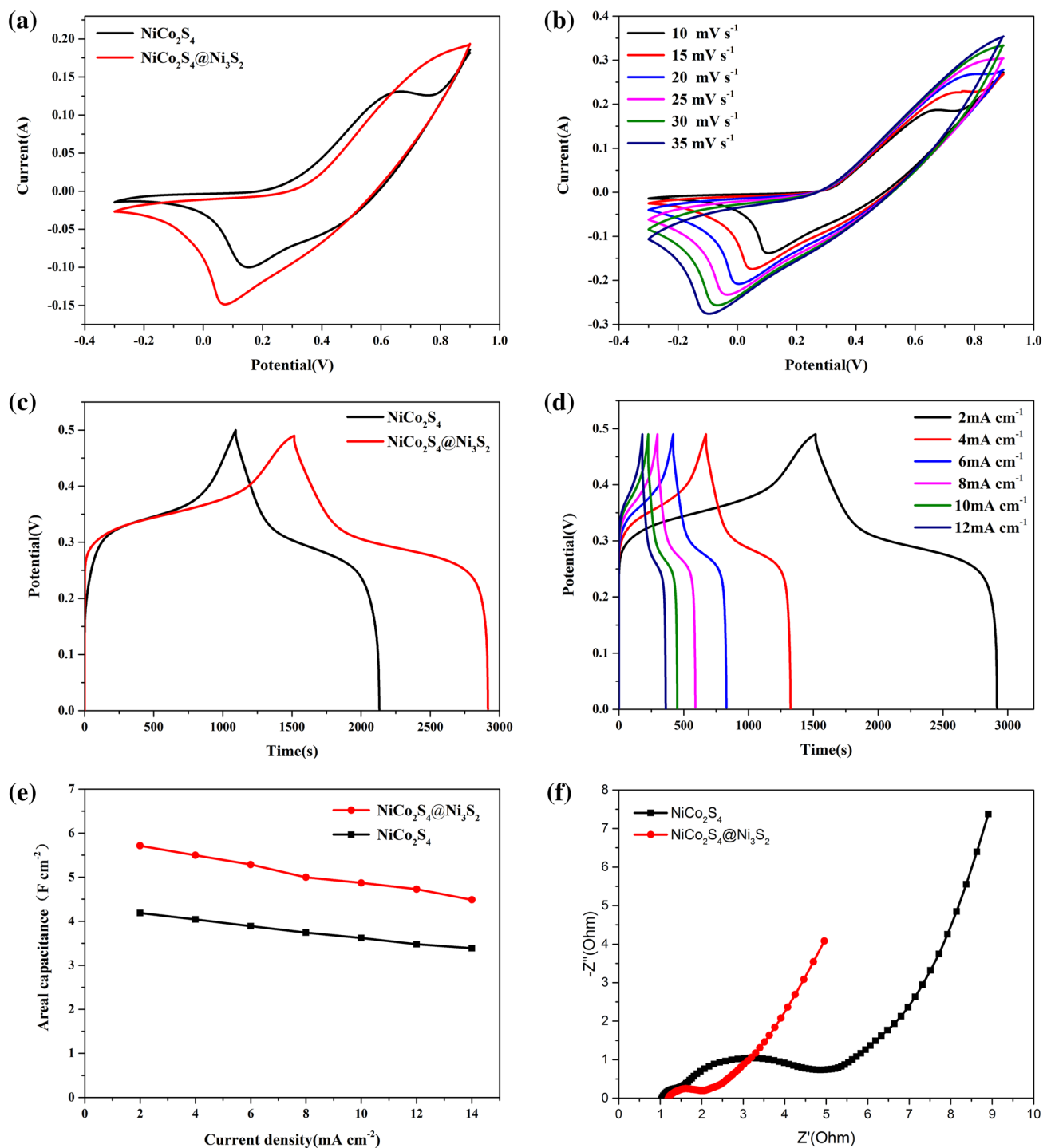


Fig. 7 a CV curves of the NiCo_2S_4 and $5\text{-NiCo}_2\text{S}_4$ @ Ni_3S_2 at scan of 10 mV/s . b CV curves after electrodeposition at various scan rates. c Charge-discharge curves of the NiCo_2S_4 and $5\text{-NiCo}_2\text{S}_4$ @ Ni_3S_2 . d Charge-discharge curves after Electrodeposition at various cur-

rent densities. e Specific capacitance as a function of current density during the activation process. f Nyquist plots of the NiCo_2S_4 and $5\text{-NiCo}_2\text{S}_4$ @ Ni_3S_2

not change significantly, implying that the reversible electrochemical redox reaction process still occurs as the scan rate changes [18].

It calculates the corresponding specific capacitance of charge and discharge from the GCD curves, which evaluated the potential of electrode materials in supercapacitor applications. The detailed specific capacitance of samples are calculated by the following equation [46, 47], where C_s ($F\text{ cm}^{-2}$) is the specific capacitance, I (A) is the current density, Δt (s) is the discharge time, Δv (V) is the voltage window and S (cm^2) is surface area of the product.

$$C_s = \frac{I \times \Delta t}{\Delta v \times S} \quad (3)$$

To further evaluate the electrochemical performance of NiCo_2S_4 nanorod arrays and $\text{NiCo}_2\text{S}_4@ \text{Ni}_3\text{S}_2$ core/shell nanorod arrays, the charge–discharge tests in the potential range between 0 and 0.5 V at the same current density of 2 mA cm^{-2} confirmed improved capacitance. We can easily see from Fig. 7c, the $\text{NiCo}_2\text{S}_4@ \text{Ni}_3\text{S}_2$ core/shell nanorod arrays electrode delivers a much longer charge–discharge time than the bare NiCo_2S_4 and calculate that the specific capacitances of NiCo_2S_4 and $\text{NiCo}_2\text{S}_4@ \text{Ni}_3\text{S}_2$ are 5.714 F cm^{-2} and 4.408 F cm^{-2} at 2 mA cm^{-2} , respectively. The close contact of the $\text{NiCo}_2\text{S}_4@ \text{Ni}_3\text{S}_2$ core–shell structure not only shortens the road force of electron transport, but also increases more reactive sites, resulting in improved electrochemical performance [36]. As observed in the CV curve, we also see the corresponding platform in the GCD curve, indicating that the sample all exhibit pseudocapacitance behavior [48]. Figure 7d shows the galvanostatic charge/discharge curves in the potential range of 0–0.5 V at various current densities. Moreover, based on the GCD curve, the specific capacitance of the sample at different current density is calculated Fig. 7e, the specific capacitance values calculated for $\text{NiCo}_2\text{S}_4@ \text{Ni}_3\text{S}_2$ are 5.704, 5.33, 5.045, 4.805, 4.579 and 4.425 mF cm^{-2} at 2, 4, 6, 8, 10 and 12 mA cm^{-2} , respectively, where the NiCo_2S_4 and $\text{NiCo}_2\text{S}_4@ \text{Ni}_3\text{S}_2$ core/shell nanorod arrays electrode exhibits superior rate performance.

EIS test was performed to further understand the change of electrochemical performance with the frequency range from 0.01 Hz to 100 kHz. We can clearly see from Fig. 7f that the intersection of Nyquist plots with the horizontal axis revealed $\text{NiCo}_2\text{S}_4@ \text{Ni}_3\text{S}_2$ and NiCo_2S_4 electrode have almost the same internal resistances of the electrode (R_s), which means that the contact resistance between the active electrode material and the carbon cloth interface, and the intrinsic resistance of the electrode materials are small [49]. In addition, a smaller semicircle indicates a smaller interfacial charge transfer impedance (R_{ct}), confirming that $\text{NiCo}_2\text{S}_4@ \text{Ni}_3\text{S}_2$ has a much lower interfacial charge transfer resistance [50, 51]. Furthermore, a smaller slope of the slash

line at the low-frequency region corresponds to $\text{NiCo}_2\text{S}_4@ \text{Ni}_3\text{S}_2$ nanorod arrays has a smaller Warburg resistance (Z_w), indicating that the smaller diffusion resistance of the ions in the electrode material $\text{NiCo}_2\text{S}_4@ \text{Ni}_3\text{S}_2$ core/shell nanorod arrays [52]. Totally, the total resistance of $\text{NiCo}_2\text{S}_4@ \text{Ni}_3\text{S}_2$ is smaller than the bare NiCo_2S_4 , which is one of the reasons $\text{NiCo}_2\text{S}_4@ \text{Ni}_3\text{S}_2$ core/shell nanorod arrays has better electrochemical performance [41, 53].

Notably, the charge and discharge cycle stability of Ni_3S_2 was tested at 40 mA cm^{-2} to further understand the cycle performance of the sample. As can be seen from Fig. 8, the specific capacitance of $\text{NiCo}_2\text{S}_4@ \text{Ni}_3\text{S}_2$ core/shell nanorod arrays retains 75% of the initial value after 2000 cycles while NiCo_2S_4 retains 65%. Therefore, the cycle performance is significantly increased by growing a layer of Ni_3S_2 on the surface of NiCo_2S_4 nanorod arrays.

Through the above analysis, this film-like Ni_3S_2 covering on the NiCo_2S_4 nanorod arrays not only greatly increases the reaction site of NiCo_2S_4 but also forms a special synergistic effect. The high specific surface area provides considerable capacitance and the special structure reduce the path of ion transport, which is known to be one of the reasons for improving its electrochemical performance [54]. These results imply that the $\text{NiCo}_2\text{S}_4@ \text{Ni}_3\text{S}_2$ core/shell nanorod arrays as active electrode materials will be one of the promising candidates for supercapacitor applications.

5.3 Electrochemical performances of the assembled asymmetric supercapacitor (ASC)

As can be seen from Fig. 9a, the $\text{NiCo}_2\text{S}_4@ \text{Ni}_3\text{S}_2$ nanorod array electrode was used as the positive electrode material and Fe_2O_3 was used as the negative electrode material to

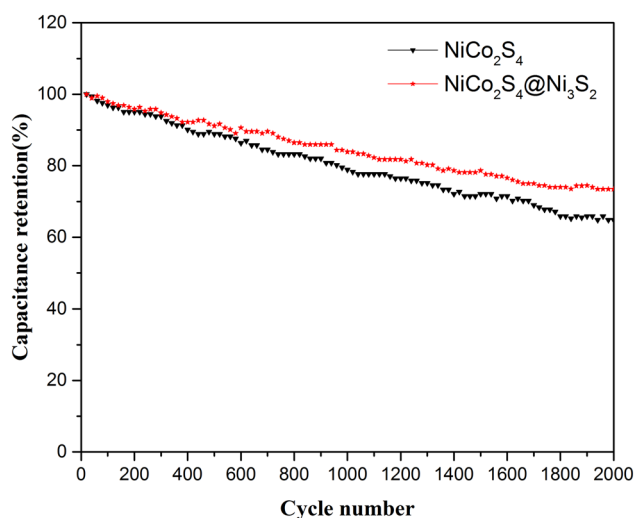


Fig. 8 Cycling performance of the NiCo_2S_4 and $5\text{-NiCo}_2\text{S}_4@ \text{Ni}_3\text{S}_2$ at a current density of 10 mA cm^{-2}

assemble the supercapacitor. According to the equilibrium relationship between the charge $q_+ = q_-$ between the positive electrode and the negative electrode, the corresponding mass of the positive and negative electrodes can be weighed. The formula is as follows:

$$\frac{m_+}{m_-} = \frac{C_- \times V_+}{C_+ \times V_-} \quad (4)$$

m_+ (mg) and m_- (mg) are the masses of positive and negative active respectively, C_+ ($F g^{-1}$), C_- ($F g^{-1}$), V_+ (V),

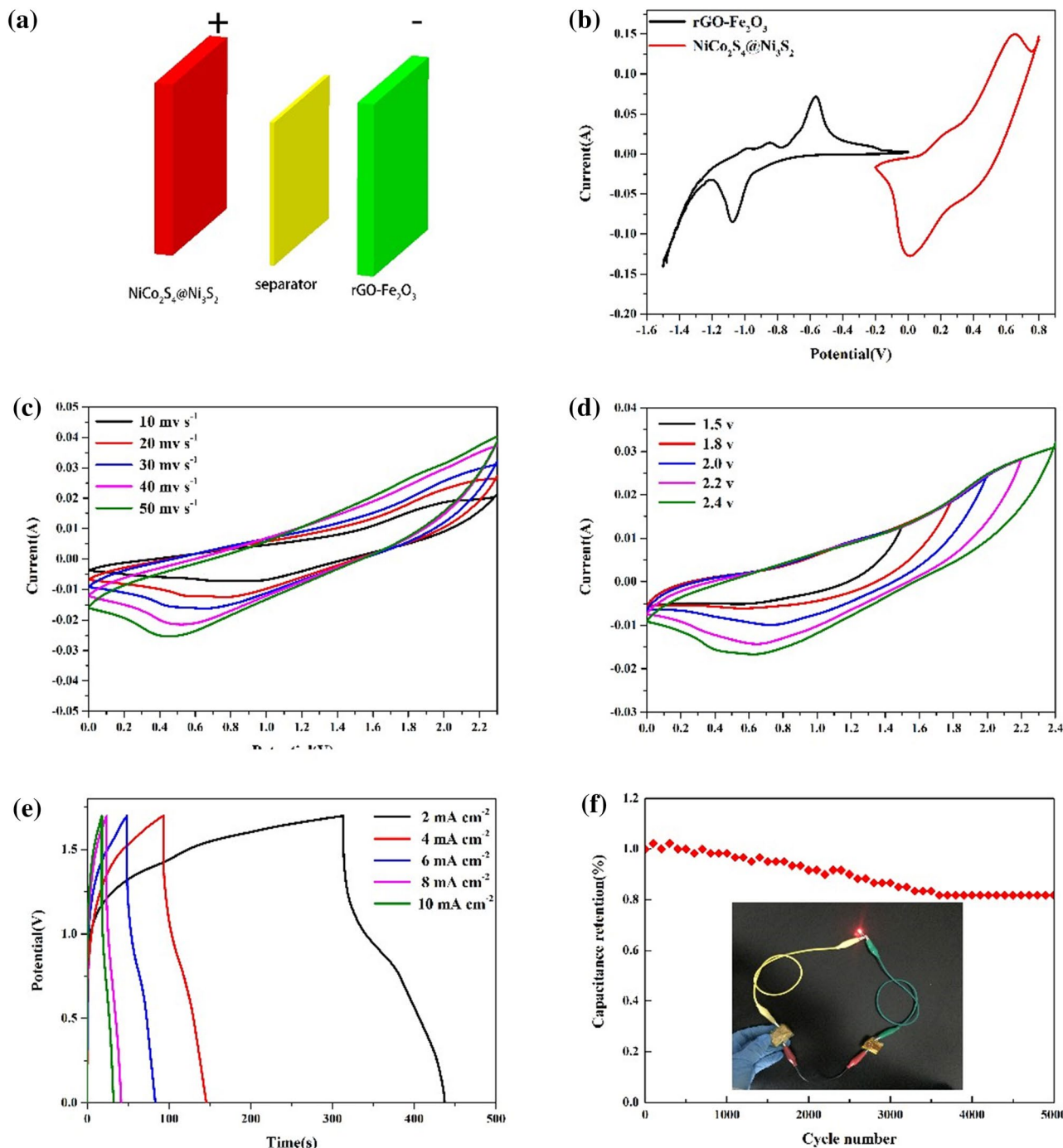


Fig. 9 **a** The structural illustration of the asymmetric supercapacitor based on the $NiCo_2S_4@Ni_3S_2$ and $rGo-Fe_2O_3$. **b** CV curves of $NiCo_2S_4@Ni_3S_2/rGo-Fe_2O_3$ ASC at a scan rate of 30 mV/s. **c** CV curves of $NiCo_2S_4@Ni_3S_2/rGo-Fe_2O_3$ ASC at various scan rates. **d** CV curves of $NiCo_2S_4@Ni_3S_2/rGo-Fe_2O_3$ ASC at scan rate of 50 mV/s at different working voltages. **e** Charge–discharge curves of the $NiCo_2S_4@Ni_3S_2/rGo-Fe_2O_3$ ASC at various current densities. **f** Cycling performance of the $NiCo_2S_4@Ni_3S_2/rGo-Fe_2O_3$ ASC

d CV curves of $NiCo_2S_4@Ni_3S_2/rGo-Fe_2O_3$ ASC at scan rate of 50 mV/s at different working voltages. **e** Charge–discharge curves of the $NiCo_2S_4@Ni_3S_2/rGo-Fe_2O_3$ ASC at various current densities. **f** Cycling performance of the $NiCo_2S_4@Ni_3S_2/rGo-Fe_2O_3$ ASC

V_- (V) is their corresponding specific capacitance and voltage window.

The CV curve of $\text{NiCo}_2\text{S}_4@/\text{Ni}_3\text{S}_2$ and AC electrodes collected in the 2 M KOH electrolyte in a three-electrode system, with voltage windows of -1.5 to 0 V and -0.3 to 0.8 V, is demonstrated in Fig. 9b. Figure 9c shows the CV curve of $\text{NiCo}_2\text{S}_4@/\text{Ni}_3\text{S}_2//\text{rGo-Fe}_2\text{O}_3$ ASC at different voltage windows at 30 mV s^{-1} . As the sweep speed increases, the shape of the CV curve does not change significantly, suggesting a good rate capability [47]. Figure 9d shows the CV curve of the $\text{NiCo}_2\text{S}_4@/\text{Ni}_3\text{S}_2//\text{rGo-Fe}_2\text{O}_3$ device recorded at various voltage windows of 1.5 to 2.4 V were ascribed to the oxidation reactions between the electrolyte and the active electrode. Figure 9e shows the galvanostatic charge/discharge curves for different current densities from 1 to 15 mA cm^{-2} in the potential window of 0 – 1.7 V, which makes it easy to calculate specific capacitance of $\text{NiCo}_2\text{S}_4@/\text{Ni}_3\text{S}_2//\text{rGo-Fe}_2\text{O}_3$ are 155 mF cm^{-2} at 2 mA cm^{-2} and 85.2 mF cm^{-2} at 20 mA cm^{-2} . Small voltage drops at various current densities with a symmetric charge discharge curves indicate good electrochemical behaviors and superb electrochemical reversibility. As shown in Fig. 9f, the $\text{NiCo}_2\text{S}_4@/\text{Ni}_3\text{S}_2//\text{rGo-Fe}_2\text{O}_3$ ASC was cycled 5000 cycles at a current density of 40 mA cm^{-2} to evaluate the cycle performance of the ASC unit. After 5000 cycles, the capacitance remains above 72% of the initial capacity, which means ASC has better cycle stability. Power density and energy density are two important bases for characterizing the performance of electrochemical supercapacitors. It has been calculated that the $\text{NiCo}_2\text{S}_4@/\text{Ni}_3\text{S}_2//\text{rGo-Fe}_2\text{O}_3$ ASC unit has an energy density of 5.9 mWh cm^{-3} at a power density of 171 mW cm^{-3} according to formulas (1) and (2), which is competitive in the current study. Such as MnO_2/ZnO graphene-ASCs ($0.234 \text{ mWh cm}^{-3}$, 0.134 W cm^{-3}) [55], MnO_2 nanorods (0.25 mWh cm^{-3}) [56].

6 Conclusions

In summary, we use two-step hydrothermal and electrodeposition method to grow Ni_3S_2 film on NiCo_2S_4 rod to form a flexible core–shell structure. Since NiCo_2S_4 and Ni_3S_2 form this particular structure, the electrochemical performance of $\text{NiCo}_2\text{S}_4@/\text{Ni}_3\text{S}_2$ nanorod arrays as a supercapacitor electrode material are 5.714 F cm^{-2} at 2 mA cm^{-2} and 4.408 F cm^{-2} at 10 mA cm^{-2} , which is much higher than that of pure NiCo_2S_4 electrode. The close contact of the $\text{NiCo}_2\text{S}_4@/\text{Ni}_3\text{S}_2$ core–shell structure not only shortens the road force of electron transport, but also increases more reactive sites, resulting in improved electrochemical performance. The asymmetric supercapacitor with $\text{NiCo}_2\text{S}_4@/\text{Ni}_3\text{S}_2$ core/shell nanorod arrays as the positive electrode and $\text{rGo-Fe}_2\text{O}_3$ as the negative electrode has an energy density of

5.9 mWh cm^{-3} at a power density of 171 mW cm^{-3} , indicating that this kind of electrode material has great potential in the application of energy storage equipment.

Acknowledgements This work is primarily supported by National Natural Science Foundation of China (51871238, 51671214), Xuzhou Science and Technology Project (KC18075) and Postgraduate Teaching Reform Project (YJSJG-2018-003).

References

1. M. Mastragostino, C. Arbizzani, F. Soavi, Conducting polymers as electrode materials in supercapacitors. *Solid State Ion.* **148**, 493–498 (2002)
2. J. Bae, M.K. Song, Y.J. Park, J.M. Kim, M. Liu, Z.L. Wang, Fiber supercapacitors made of nanowire–fiber hybrid structures for wearable/flexible energy storage. *Angew. Chem. Int. Ed.* **50**, 1683–1687 (2011)
3. X. Lu, M. Yu, G. Wang, Y. Tong, Y. Li, Flexible solid-state supercapacitors: design, fabrication and applications. *Energy Environ. Sci.* **7**, 216–2181 (2014)
4. L. Zhang, X. Hu, Z. Wang, F. Sun, D.G. Dorrell, A review of supercapacitor modeling, estimation, and applications: a control/management perspective. *Renew. Sustain. Energy Rev.* **81**, 1868–1878 (2018)
5. C. Shao, T. Xu, J. Gao, Y. Liang, Y. Zhao, L. Qu, Flexible and integrated supercapacitor with tunable energy storage. *Nanoscale* **9**, 12324 (2017)
6. A. Pendashteh, J. Palma, M. Anderson, R. Marcilla, Nanostructured porous wires of iron cobaltite: novel positive electrode for high-performance hybrid energy storage devices. *J. Mater. Chem. A* **3**, 16849–16859 (2015)
7. J. Qi, Y. Chang, Y. Sui, Y. He, Q. Meng, F. Wei, Y. Ren, Y. Jin, Facile synthesis of Ag-decorated Ni_3S_2 nanosheets with 3D bush structure grown on rGO and its application as positive electrode material in asymmetric supercapacitor. *Adv. Mater. Interfaces* **5**, 1700985 (2018)
8. A.C. Forse, C. Merlet, J.M. Griffin, C.P. Grey, New perspectives on the charging mechanisms of supercapacitors. *J. Am. Chem. Soc.* **138**, 5731–5744 (2016)
9. A. González, E. Goikolea, J.A. Barrena, R. Mysyk, Review on supercapacitors: technologies and materials. *Renew. Sustain. Energy Rev.* **58**, 1189–1206 (2016)
10. J. Bae, Y.J. Park, M. Lee, S.N. Cha, Y.J. Choi, C.S. Lee, J.M. Kim, Z.L. Wang, Single-fiber-based hybridization of energy converters and storage units using graphene as electrodes. *Adv. Mater.* **23**, 3446–3449 (2011)
11. X. Liu, G. Chen, H. Guan, C. Dong, X. Xiao, Y. Wang, Binder-free $\text{NiO}@\text{MnO}_2$ core–shell electrode: rod-like NiO core prepared through corrosion by oxalic acid and enhanced pseudocapacitance with sphere-like MnO_2 shell. *Electrochim. Acta* **189**, 83–92 (2016)
12. A.E. Reddy, T. Anitha, C.V.V.M. Gopi, S. Srinivasa Rao, C.V. Thulasi-Varma, D. Punnoose, H. Kim, Fabrication of a snail shell-like structured $\text{MnO}_2@/\text{CoNiO}_2$ composite electrode for high performance supercapacitors. *RSC Adv.* **7**, 1231–1238 (2017)
13. M. Huang, F. Li, X.L. Zhao, D. Luo, X.Q. You, Y.X. Zhang, G. Li, Hierarchical $\text{ZnO}@\text{MnO}_2$ core–shell pillar arrays on Ni foam for binder-free supercapacitor electrodes. *Electrochim. Acta* **152**, 172–177 (2015)
14. J. Hao, S. Peng, H. Li, S. Dang, T. Qin, Y. Wen, J. Huang, F. Ma, D. Gao, F. Li, G. Cao, A low crystallinity oxygen-vacancy-rich

- Co₃O₄ cathode for high-performance flexible asymmetric supercapacitors. *J. Mater. Chem. A* **6**, 16094–16100 (2018)
15. Z. Zhu, Y. Zhou, S. Wang, C. Zhao, Z. Li, G. Chen, C. Zhao, Ni counterpart-assisted synthesis of nanoarchitected Co₃O₄/CoS/Ni(OH)₂@Co electrode for superior supercapacitor. *Electrochim. Acta* **284**, 444–453 (2018)
 16. R.M. Kore, B.J. Lokhande, A robust solvent deficient route synthesis of mesoporous Fe₂O₃ nanoparticles as supercapacitor electrode material with improved capacitive performance. *J. Alloy. Compd.* **725**, 129–138 (2017)
 17. S.N. Khataavkar, S.D. Sartale, Alpha-Fe₂O₃ thin films by liquid phase deposition: low-cost option for supercapacitor. *J. Solid State Electron.* **21**, 2555–2566 (2017)
 18. G. Liu, B. Wang, T. Liu, L. Wang, H. Luo, T. Gao, F. Wang, A. Liu, D. Wang, 3D self-supported hierarchical core/shell structured MnCo₂O₄@CoS arrays for high-energy supercapacitors. *J. Mater. Chem. A* **6**, 1822–1831 (2018)
 19. W. Liu, J. Zhang, Z. Bai, G. Jiang, M. Li, K. Feng, L. Yang, Y. Ding, T. Yu, Z. Chen, A. Yu, Controllable urchin-like NiCo₂S₄ microsphere synergized with sulfur-doped graphene as bifunctional catalyst for superior rechargeable Zn-air battery. *Adv. Funct. Mater.* **28**, 1706675 (2018)
 20. Q. Wang, X. Wang, J. Xu, X. Ouyang, X. Hou, D. Chen, R. Wang, G. Shen, Flexible coaxial-type fiber supercapacitor based on NiCo₂O₄ nanosheets electrodes. *Nano Energy* **8**, 44–51 (2014)
 21. J. Yang, M. Ma, C. Sun, Y. Zhang, W. Huang, X. Dong, Hybrid NiCo₂S₄@MnO₂ heterostructures for high-performance supercapacitor electrodes. *J. Mater. Chem. A* **3**, 1258–1264 (2014)
 22. X. Zhang, C. Si, X. Guo, R. Kong, F. Qu, A MnCo₂S₄ nanowire array as an earth-abundant electrocatalyst for an efficient oxygen evolution reaction under alkaline conditions. *J. Mater. Chem. A* **5**, 17211–17215 (2017)
 23. A.M. Elshahawy, X. Li, H. Zhang, Y. Hu, K.H. Ho, C. Guan, J. Wang, Controllable MnCo₂S₄ nanostructures for high performance hybrid supercapacitors. *J. Mater. Chem. A* **5**, 7494–7506 (2017)
 24. M. Tong, L. Wang, P. Yu, C. Tian, X. Liu, W. Zhou, H. Fu, Ni₃S₂ nanosheets in situ epitaxially grown on nanorods as high active and stable homojunction electrocatalyst for hydrogen evolution reaction. *ACS Sustain. Chem. Eng.* **6**, 2474–2481 (2017)
 25. Y. Gong, H. Pan, Z. Xu, Z. Yang, Y. Lin, J. Wang, Crossed FeCo₂S₄ nanosheet arrays grown on 3D nickel foam as high-efficient electrocatalyst for overall water splitting. *Int. J. Hydrogen Energy* **43**, 17259–17264 (2018)
 26. C. Deng, L. Yang, C. Yang, P. Shen, L. Zhao, Z. Wang, C. Wang, J. Li, D. Qian, Spinel FeCo₂S₄ nanoflower arrays grown on Ni foam as novel binder-free electrodes for long-cycle-life supercapacitors. *Appl. Surf. Sci.* **428**, 148–153 (2018)
 27. K. Krishnamoorthy, G.K. Veerasubramani, S. Radhakrishnan, S.J. Kim, One pot hydrothermal growth of hierarchical nanostructured Ni₃S₂ on Ni foam for supercapacitor application. *Chem. Eng. J.* **251**, 116–122 (2014)
 28. Z. Zhang, Z. Huang, L. Ren, Y. Shen, X. Qi, J. Zhong, One-pot synthesis of hierarchically nanostructured Ni₃S₂ dendrites as active materials for supercapacitors. *Electrochim. Acta* **149**, 316–323 (2014)
 29. J. Wang, D. Chao, J. Liu, L. Li, L. Lai, J. Lin, Z. Shen, Ni₃S₂@MoS₂ core/shell nanorod arrays on Ni foam for high-performance electrochemical energy storage. *Nano Energy* **7**, 151–160 (2014)
 30. X. Zhu, X. Jiang, X. Liu, L. Xiao, X. Ai, H. Yang, Y. Cao, Amorphous CoS nanoparticle/reduced graphene oxide composite as high-performance anode material for sodium-ion batteries. *Ceram. Int.* **43**, 9630–9635 (2017)
 31. R. Wang, Y. Sui, S. Huang, Y. Pu, P. Cao, High-performance flexible all-solid-state asymmetric supercapacitors from nanostructured electrodes prepared by oxidation-assisted dealloying protocol. *Chem. Eng. J.* **331**, 527–535 (2018)
 32. D. Shi, L. Zhang, X. Yin, T.J. Huang, H. Gong, A one step processed advanced interwoven architecture of Ni(OH)₂ and Cu nanosheets with ultrahigh supercapacitor performance. *J. Mater. Chem. A* **4**, 12144–12151 (2016)
 33. J. Lin, Y. Wang, X. Zheng, H. Liang, H. Jia, J. Qi, J. Cao, J. Tu, W. Fei, J. Feng, P-Doped NiCo₂S₄ nanotubes as battery-type electrodes for high-performance asymmetric supercapacitors. *Dalton Trans.* **47**, 8771–8778 (2018)
 34. R. Li, S. Wang, Z. Huang, F. Lu, T. He, NiCo₂S₄@Co(OH)₂ core-shell nanotube arrays in situ grown on Ni foam for high performances asymmetric supercapacitors. *J. Power Sources* **312**, 156–164 (2016)
 35. X. Liu, Z. Wu, Y. Yin, Hierarchical NiCo₂S₄@PANI core/shell nanowires grown on carbon fiber with enhanced electrochemical performance for hybrid supercapacitors. *Chem. Eng. J.* **323**, 330–339 (2017)
 36. T. He, S. Wang, F. Lu, M. Zhang, X. Zhang, L. Xu, Controllable synthesis of hierarchical NiCo₂S₄@Ni₃S₂ core-shell nanotube arrays with excellent electrochemical performance for aqueous asymmetric supercapacitors. *RSC Adv.* **6**, 97352–97362 (2016)
 37. X. Liu, F. Wei, Y. Sui, J. Qi, Y. He, Q. Meng, Polyhedral ternary oxide FeCo₂O₄: a new electrode material for supercapacitors. *J. Alloy. Compd.* **735**, 1339–1343 (2018)
 38. Z. Ma, X. Huang, S. Dou, J. Wu, S. Wang, One-pot synthesis of Fe₂O₃ nanoparticles on nitrogen-doped graphene as advanced supercapacitor electrode materials. *J. Phys. Chem. C* **118**, 17231–17239 (2014)
 39. H. Quan, B. Cheng, Y. Xiao, S. Lei, One-pot synthesis of α-Fe₂O₃ nanoplates-reduced graphene oxide composites for supercapacitor application. *Chem. Eng. J.* **286**, 165–173 (2016)
 40. D. Kong, C. Cheng, Y. Wang, J.I. Wong, Y. Yang, H.Y. Yang, Three-dimensional Co₃O₄@C@Ni₃S₂ sandwich-structured nanoneedle arrays: towards high-performance flexible all-solid-state asymmetric supercapacitors. *J. Mater. Chem. A* **3**, 16150–16161 (2015)
 41. M. Liang, M. Zhao, H. Wang, J. Shen, X. Song, Enhanced cycling stability of hierarchical NiCo₂S₄@Ni(OH)₂@PPy core-shell nanotube arrays for aqueous asymmetric supercapacitors. *J. Mater. Chem. A* **6**, 2482–2493 (2018)
 42. Y. Wang, J. Zhong, F. Ding, Q. Zhao, Z. Zhang, X. Liu, Y. Liu, H. Rao, P. Zou, X. Wang, A bifunctional NiCo₂S₄/reduced graphene oxide@polyaniline nanocomposite as a highly-efficient electrode for glucose and rutin detection. *New J. Chem.* **42**, 9398–9409 (2018)
 43. J. Peng, J. Xu, Z. Wang, Z. Ding, S. Wang, Developing an efficient NiCo₂S₄ cocatalyst for improving the visible light H₂ evolution performance of CdS nanoparticles. *Phys. Chem. Chem. Phys.* **19**, 25919–25926 (2017)
 44. B. Li, J. Xia, J. Liu, Q. Liu, G. Huang, H. Zhang, X. Jing, R. Li, J. Wang, RGO nanosheets modified NiCo₂S₄ nanoflowers for improved ethanol sensing performance at low temperature. *Chem. Phys. Lett.* **703**, 80–85 (2018)
 45. D. Li, Y. Gong, C. Pan, Facile synthesis of hybrid CNTs/NiCo₂S₄ composite for high performance supercapacitors. *Sci. Rep.* **6**, 29788 (2016)
 46. P. Howli, S. Das, S. Sarkar, M. Samanta, K. Panigrahi, N.S. Das, K.K. Chattopadhyay, Co₃O₄ nanowires on flexible carbon fabric as a binder-free electrode for all solid-state symmetric supercapacitor. *ACS Omega* **2**, 4216–4226 (2017)
 47. A. Ramadoss, S.J. Kim, Hierarchically structured TiO₂@MnO₂ nanowall arrays as potential electrode material for high-performance supercapacitors. *Int. J. Hydrogen Energy* **39**, 12201–12212 (2014)

48. H. Chen, X.L. Liu, J.M. Zhang, F. Dong, Y.X. Zhang, Rational synthesis of hybrid NiCo₂S₄@MnO₂ heterostructures for supercapacitor electrodes. *Ceram. Int.* **42**, 8909–8914 (2016)
49. Y. Zheng, J. Xu, X. Yang, Y. Zhang, Y. Shang, X. Hu, Decoration NiCo₂S₄ nanoflakes onto Ppy nanotubes as core–shell heterostructure material for high-performance asymmetric supercapacitor. *Chem. Eng. J.* **333**, 111–121 (2018)
50. S. Ghasemi, S.R. Hosseini, O. Boore-talari, Sonochemical assisted synthesis MnO₂/RGO nanohybrid as effective electrode material for supercapacitor. *Ultrason. Sonochem.* **40**, 675–685 (2018)
51. S. Sarkar, P. Howli, U.K. Ghorai, B. Das, M. Samanta, N.S. Das, K.K. Chattopadhyay, Flower-like Cu₂NiSnS₄ microspheres for application as electrodes of asymmetric supercapacitors endowed with high energy density. *CrystEngComm* **20**, 1443–1454 (2018)
52. L. Li, K.S. Hui, K.N. Hui, Y. Cho, Ultrathin petal-like NiAl layered double oxide/sulfide composites as an advanced electrode for high-performance asymmetric supercapacitors. *J. Mater. Chem. A* **5**, 19687–19696 (2017)
53. S. Ibrahim, H. Darwish, M.M. Goma, Electrical and physico-chemical properties of some Ag₂O-containing lithia iron silica phosphate glasses. *J. Mater. Sci.* **23**, 1131–1142 (2012)
54. Q. Chen, J. Li, C. Liao, G. Hu, Y. Fu, O.K. Asare, S. Shi, Z. Liu, L. Zhou, L. Mai, Ni foam supported NiO nanosheets as high-performance free-standing electrodes for hybrid supercapacitors and Ni–Zn batteries. *J. Mater. Chem. A* **6**, 19488–19494 (2018)
55. W. Zilong, Z. Zhu, J. Qiu, S. Yang, High performance flexible solid-state asymmetric supercapacitors from MnO₂/ZnO core–shell nanorods/specially reduced graphene oxide. *J. Mater. Chem. C* **2**, 1331–1336 (2014)
56. T. Zhai, S. Xie, M. Yu, P. Fang, C. Liang, X. Lu, Y. Tong, Oxygen vacancies enhancing capacitive properties of MnO₂ nanorods for wearable asymmetric supercapacitors. *Nano Energy* **8**, 255–263 (2014)

Publisher's Note Springer Nature remains neutral with regard to jurisdictional claims in published maps and institutional affiliations.